IEEE Photonics Journal
An IEEE Photonics Society Publication

Open Access

Performance Analysis and Power Optimization for Spectrum-Sharing Mixed RF/FSO Relay Networks With Energy Harvesting

Volume 11, Number 2, April 2019

Ahmed H. Abd El-Malek, *Member, IEEE*
Mohamed A. Aboulhassan, *Member, IEEE*
Anas M. Salhab, *Senior Member, IEEE*
Salam A. Zummo, *Senior Member, IEEE*

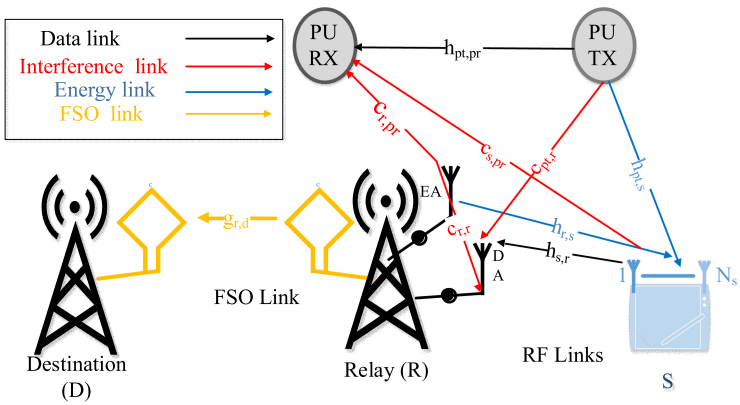

DOI: 10.1109/JPHOT.2019.2897837
1943-0655 © 2019 IEEE

IEEE photonics SOCIETY

IEEE

Performance Analysis and Power Optimization for Spectrum-Sharing Mixed RF/FSO Relay Networks With Energy Harvesting

Ahmed H. Abd El-Malek,[1] ***Member, IEEE***,
Mohamed A. Aboulhassan,[2] ***Member, IEEE***,
Anas M. Salhab,[3] ***Senior Member, IEEE***,
and Salam A. Zummo,[3] ***Senior Member, IEEE***

[1]School of Electronics, Communications and Computer Engineering, Egypt–Japan University of Science and Technology, Alexandria 21934, Egypt
[2]Department of Electrical Engineering, Pharos University in Alexandria, Alexandria 21311, Egypt
[3]Department of Electrical Engineering, King Fahd University of Petroleum and Minerals, Dhahran 31261, Saudi Arabia

DOI:10.1109/JPHOT.2019.2897837

Manuscript received December 27, 2018; revised January 31, 2019; accepted February 2, 2019. Date of publication February 6, 2019; date of current version February 26, 2019. This work was supported in part by the National Plan for Science, Technology and Innovation King Abdulaziz City for Science and Technology through the Science and Technology Unit at King Fahd University of Petroleum and Minerals (KFUPM) the Kingdom of Saudi Arabia under Grant 15-ELE4157-04, and in part by the Deanship of Scientific Research in KFUPM under Grant IN161023. Corresponding authors: Salam A. Zummo and Anas M. Salhab (e-mail: zummo@kfupm.edu.sa; salhab@kfupm.edu.sa).

Abstract: In this paper, the energy harvesting in mixed multiple-input-single-output radio frequency (RF)/free space optical (FSO) networks is studied. Assuming underlay mode, the secondary user (SU) source with limited battery communicates with its destination via a hybrid SU relay. The SU source harvests energy from both the hybrid relay and the primary network. The hybrid SU relay node is equipped with two antennas; one for energy transmission to the secondary user and the other for data reception. The SU source transmits its data over an RF link to the relay. Then, the relay decodes the SU data before retransmitting it to the SU destination over an optical link. The RF/FSO channels are assumed to follow Nakagami-m/Málaga-$\mathcal{M}$ fading models with pointing errors on the FSO link. Closed-form expressions for the exact outage probability, average bit error rate, and ergodic capacity are derived. For high signal-to-noise ratio values, closed-form expressions for the asymptotic outage probability and average bit error rate are derived. Based on the asymptotic results, a power allocation model is proposed to enhance the system outage performance. Some simulation and numerical results are employed to validate the derived expressions.

Index Terms: Free space optical communications, cognitive radio, multiple antennas, energy harvesting, outage probability, ergodic capacity.

1. Introduction

The multi-hop networks are considered as one of the promising networking solutions for providing reliable transmission of data. In order to achieve the best benefits of multiple links, different types

of links can be used jointly such as mixed radio frequency/free space optical (RF/FSO) links. FSO is considered as an efficient technology that can be used to fulfill the dramatic high demand for improved throughputs. It aims to provide higher data rates and cost-efficient solution for unlicensed spectrum compared to conventional RF links [1]. Therefore, using both the RF and FSO technologies leads to a significant enhancement in communication networks performance.

Energy harvesting (EH) and cognitive radio (CR) techniques are considered as one of the promising trends in RF technology that have been investigated extensively. EH technology aims to transmit the power to smart devices over wireless links [2], [3], while CR is a well-known technology which studies the improvement of spectrum utilization efficiency. Therefore, merging such trends with FSO transmission represents a promising solution for satisfying nowadays very high data rate applications. In [4], [5], the secondary user (SU) harvests energy from the primary users (PU) and uses the harvested energy for data transmission, however there is no dedicated power station for energy harvesting. Whereas, in [6], energy-harvesting-aided spectrum sensing is proposed where the SU senses the presence of the PU and harvests energy from it. Then, a multi-objective optimization problem is formulated.

Various research works studied the primary performance metrics of FSO links such as bit error rate (BER), outage probability, and ergodic capacity. In [7], the outage probability, BER, and the average capacity of all-optical FSO networks were studied. Recently, the Málaga-$\mathcal{M}$ [8] distribution was proposed as an efficient model to describe the behavior of optical wave propagation, instead of conventional models such as log-normal and Gamma-Gamma distributions [9].

The usage of EH techniques in relay networks was studied before in several research works. In [10], analytical expressions for the outage probability and overall throughput in a decode-and-forward (DF) EH relaying network were derived. The main aspects of wireless links incorporated with EH techniques have been intensively studied in literature. Throughput maximization was studied in [11] and [12]. In [11], the secondary user (SU) throughput was maximized through splitting the harvested and transmitted energies over time. While in [12], an algorithm was proposed to find the optimal harvesting-access policy using the value iteration, then the relationship between the throughput, the available energy in the battery, and the battery capacity were investigated. In [13], a cooperative spectrum sensing scheme in CR environment with SUs was designed based on game theory techniques. Multichannel selection techniques were studied in [14] where a multichannel selection strategy was proposed for RF-EH-CRN by maximizing SUs throughput. The power allocation problem was investigated in [15], by maximizing the average throughput finite time duration. The optimization problem was modeled as a Markov decision process with a continuous state. The work in [16] studied the throughput of SU that depends only on harvested energy. Spectrum sensing and optimum harvesting energy were investigated jointly in [17].

Devices equipped with multiple antennas were actively examined. The work in [18] studied the performance of EH-based multiple-input multiple-output (MIMO) relay systems over Nakagami-*m* fading channels, where closed-form expressions for the probability density function (pdf) and cumulative distribution function (CDF) of the signal-to-noise ratio (SNR) were calculated.

The merging of the FSO technology with the existing RF counterparts was investigated before in various research works [9], [19]–[21]. In [19], the ergodic capacity and outage probability of relay-assisted mixed FSO/RF transmission were derived assuming mixed Málaga-$\mathcal{M}/\kappa-\mu$ shadowed fading distributions, while in [9] and [20], closed-form expressions for the outage probability and bit error probability in mixed RF/FSO systems employing Nakagami-*m* fading model for the RF link were calculated. Bit error probability was also studied in [21] with a single source, single destination, and multiple relays network. The RF behavior was modeled as Nakagami-*m* fading distribution while the FSO link behavior was modeled as Gamma-Gamma scintillation. The effect of RF interference on the performance of mixed FSO/RF relay networks was analyzed in [20].

Recently, the performance of underlay CR with mixed RF/FSO networks has been investigated in many works in the literature [22]–[26]. The works in [22] investigated the performance of CR mixed RF/FSO systems under the constraints of PU interference threshold and maximum SU transmitted power where closed-form expression of the asymptotic outage probability was derived. The authors in [23] studied the impact of different interference reduction techniques on the performance of

underlay CR mixed RF/FSO networks. Whereas, the effects of nodes mobility and outdated channel state information on such networks performance were presented in [25], [26]. In addition, the works in [27], [28] investigated the multiuser scheduling scheme in underlay CR mixed RF/FSO networks in terms of outage probability, average symbol error probability, and ergodic capacity.

Motivated by the aforementioned discussion, and to the best of our knowledge, there is no previous work discusses the impact of cooperative CR network combined with EH technologies on the performance of mixed RF/FSO networks. Hence, this work studies the performance of spectrum-sharing mixed MISO RF/FSO system with EH. On the RF link, the SU equipped with multiple antennas, harvests energy from the hybrid relay node (HRN) and the primary network. Then, the SU employs the harvested energy to send its data to the HRN in the uplink transmission. The relay node decodes the SU data before transmitting it to the SU destination over a FSO link. The channel model of the RF/FSO network is assumed to follow Nakagami-m/Málaga-$\mathcal{M}$ fading models. To reduce the transmission overhead, the HRN is assumed to have no prior knowledge of the user's stored energy status. This proposed system model can be found in many practical applications such as increasing network density for real-time events, establishing of temporary wireless sensor networks, metropolitan area network extension, wireless body area networks, and connecting several smaller cells to the core network in 5G system [29]–[31]. Closed-form expressions for the system outage probability, average bit error rate (BER), and ergodic capacity are derived. Moreover, a power optimization problem is investigated to obtain the optimal downlink harvesting energy that is transmitted from the HRN to the SU. The maximization problem is formulated through minimization of the system outage probability.

The rest of this paper is organized as follows. Section 2 presents the system and channel models. The system performance measures such as outage probability, average BER, and ergodic capacity are investigated in Section 3. Section 4 presents the power optimization model. Simulation and numerical results are discussed in Section 5. Finally, conclusions are given in Section 6.

The notation used in this paper is defined as follows: Bold lower case symbols denote vectors. We use $\binom{\cdot}{\cdot}$ for the binomial coefficient, $|.|$ and $\|.\|$ represent the absolute value and the Frobenius norm of vectors, respectively. $(.)^H$ is the Hermitian (conjugate-transpose) operator of a vector input-argument. The term $f_\beta(x)$ is the pdf of random variable (RV) β, and $F_\beta(x)$ is its CDF. The function ${}_1F_1(a; b; z)$ is the hyper-geometric function, $U(a, b, z)$ is the KummerU hyper-geometric function [33], and G(.) is the Meijer G-function as defined in [34, Eq. (9.301)].

2. System and Channel Models

2.1 System Model

As shown in Figure 1, the proposed system model is a dual-hop mixed MISO RF/FSO underlay CRN in which a SU source (S) communicates with a SU destination (D) through a SU relay (R) with DF protocol in the presence of a single PU transmitter (PT) and a single PU receiver (PR). In this model, the S is equipped with multiple antennas (N_s) which are used for both energy harvesting and data transmission. Whereas, R is equipped with two RF antennas; one is the energy transmission antenna (EA), and the other one is the data reception antenna (DA). Therefore, R acts as a wireless power transmitting station to charge the nearby devices through EA, and as a data receiving station through DA. Also, R is equipped with an optical laser transmitter to communicate with D which is equipped with an optical receiver. The S harvests energy from both, the PU transmission and R. Hence, the total received power at S is given by

$$\gamma_s = \epsilon \left(P_{pt} \left\| \mathbf{h}_{pt,s} \right\|^2 + P_e \left\| \mathbf{h}_{r,s} \right\|^2 \right), \tag{1}$$

where ϵ is the energy harvesting efficiency coefficient, i.e. $0 < \epsilon < 1$; $\mathbf{h}_{pt,s}$ is a $1 \times N_s$ channel vector between PT and S, with $h_{pt,i}$ denotes the channel coefficient between PT and the i-th antenna of S with $i = 1, 2, \ldots, N_s$. Similarly, $\mathbf{h}_{r,s}$ is $1 \times N_s$ channel vector between EA and S, where $h_{r,j}$ denotes the channel coefficient between EA and the j-th antenna of S, with $j = 1, 2, \ldots, N_s$; and the powers P_{pt} and P_e represent the PT transmission power and EA transmission power, respectively. To ensure

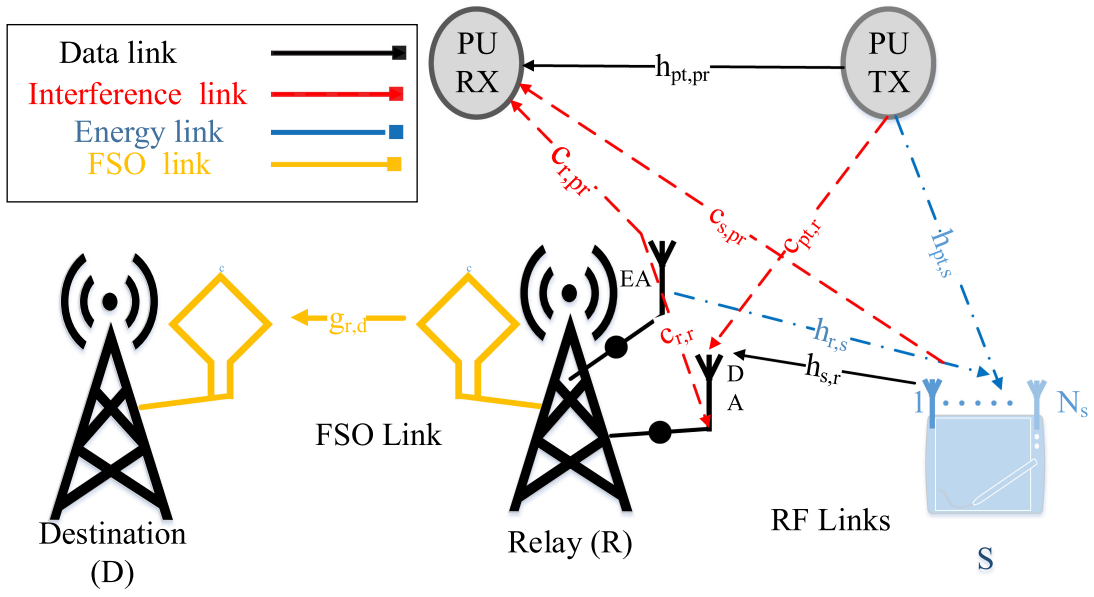

Fig. 1. Dual-hop spectrum-sharing mixed MISO RF/FSO relay network with energy harvesting.

that S is still active and alive after its data transmission, the harvested energy γ_s should be greater than an energy harvested threshold (γ_E).

For the proposed model, the communication operations take place over two time-slots. In the first time slot, S harvests energy which it uses in the second time slot to transmit its data to DA at R with a specific power P_s, which is assumed to be constant power when energy harvested exceeds γ_E. The received signal at DA suffers from co-channel interference (CCI) signals because of the simultaneous transmission of both PT and EA, and hence, the received signal at DA is given by

$$y_{s,r} = \sqrt{\frac{P_s}{N_s}}\mathbf{h}_{s,r}^H \mathbf{x}_s + \sqrt{P_{pt}}c_{pt,r}x_{pt} + \sqrt{\eta P_e}c_{r,r}x_e + w_r, \tag{2}$$

where $\mathbf{h}_{s,r} \in \mathbb{C}^{N_s \times 1}$ is the channel vector between S and R, with $h_{i,r}$ is the channel coefficient between the q-th antenna of S and R, $i = 1, 2, \ldots . N_s$; $c_{pt,r}$ denotes the CCI coefficient between PT and DA; $c_{r,r}$ denotes the self-interference channel coefficient between the two relay antennas EA and DA. The symbol vector $\mathbf{x}_s$ of size $N_s \times 1$ denotes the SU transmitted data symbols with zero mean and unit variance; x_{pt} represents the CCI signal from PT to R with zero mean and unit variance, and x_e represents the self-interference signal with zero mean and unit variance. The self-interference coefficient η represents the remaining ratio of P_e due to an imperfect self-interference cancellation process. The term w_r denotes the additive white Gaussian noise (AWGN) sample which follows a complex normal distribution with zero mean and variance of σ_0^2. The instantaneous signal-to-interference-plus-noise ratio (SINR) for the SU network over the RF links is given by

$$\gamma_{\text{RF}} = \frac{\frac{P_s}{N_s}\left\|\mathbf{h}_{s,r}\right\|^2}{P_{pt}\left|c_{pt,r}\right|^2 + \eta P_e\left|c_{r,r}\right|^2 + \sigma_0^2}. \tag{3}$$

Then, R decodes the transmitted SU data and retransmits it to D over the FSO link. Hence, the received optical signal at D is given by

$$y_{r,d} = g_{r,d}\sqrt{P_r}\widehat{x}_s + w_d, \tag{4}$$

where $g_{r,d}$ denotes the coefficient of the optical channel; $\widehat{x}_s$ denotes the decoded SU symbol by R with zero mean and unit variance which is transmitted over a FSO link with power P_r. w_d is the

AWGN sample at D with zero mean and variance σ_d^2. Hence, the SNR of the FSO link is

$$\gamma_{\text{FSO}} = \frac{P_r \left| g_{r,d} \right|^2}{\sigma_d^2}. \tag{5}$$

Finally, the instantaneous end-to-end (e2e) SINR with DF relaying protocol is given by [19]

$$\gamma_{s,d} = \min \left\{ \gamma_{\text{RF}}, \gamma_{\text{FSO}} \right\}. \tag{6}$$

2.2 Channel Models

2.2.1 For Data Transmission Over RF Links: The channel coefficients of the RF links $h_{i,j}$, for $i = 1, 2, \ldots, N_s$ and $j \in \{r, pr\}$ between the i-th antenna of S and all other nodes follow independent and identically distributed (i.i.d.) Nakagami-m fading model, the CDF of $\left\| \mathbf{h}_{s,j} \right\|^2$ (or $\left\| \mathbf{c}_{s,j} \right\|^2$) for maximal-ratio-transmission (MRT) scheme is [35]

$$F_{\left\| \mathbf{h}_{s,j} \right\|^2}(x) = 1 - \sum_{p=0}^{m_{s,j}N_s - 1} \frac{\left(m_{s,j} \lambda_{s,j} x \right)^p}{p!} \exp\left(-m_{s,j} \lambda_{s,j} x \right), \tag{7}$$

where $\lambda_{s,j} = 1/\bar{\gamma}_{s,j}$, with $\bar{\gamma}_{s,j} = \frac{P_s}{N_s \sigma_0^2} \mathbb{E}\{\|\mathbf{h}_{s,j}\|^2\} = \frac{P_s}{N_s \sigma_j^2} \Omega_{s,j}$, and $m_{s,j}$ denotes the Nakagami-m fading parameter between S and $j \in \{r, pr\}$. By differentiating (7) w.r.t. x, the pdf is given by

$$f_{\left\| \mathbf{h}_{s,j} \right\|^2}(x) = \frac{\left(m_{s,j} \lambda_{s,j} \right)^{m_{s,jN_s - 1}}}{\Gamma(m_{s,jN_s})} x^{m_{s,jN_s - 1}} \exp(-m_{s,j} \lambda_{s,j} x). \tag{8}$$

2.2.2 For Interfering Channels: For SU network, the SU signal received at DA of R suffers from two interfering signals from PT and EA of R. Variables $c_{u,r}$, $u \in \{pt, r\}$, denotes the channel links between the interferers and R which are assumed to follow independent and non-identically distributed (i.ni.d.) Nakagami-m fading model. Hence, the pdf of the total interference at the SU relay node is given by [36]

$$f_{\sum\limits_{i \in \{pt,r\}} |c_{i,r}|^2}(y) = \left[\prod_{i \in \{pt,r\}} \left(m_{i,r} \lambda_{i,r} \right)^{m_{i,r}} \right] \sum_{i \in \{pt,r\}} \exp(-m_{i,r} \lambda_{i,r} y) \sum_{j=1}^{m_{i,r}} \frac{\beta_{i,r}^{j-1} y^{m_{i,r} - j}}{(m_{i,r} - j)!(j-1)!}, \tag{9}$$

where $\beta_{i,r}^{j-1} = \frac{d^{j-1}}{ds^{j-1}} \left[\prod\limits_{\substack{v \neq i \\ v = \in \{pt,r\}}} \left(m_{v,r} \lambda_{v,r} + s \right)^{m_{v,r}} \right] \Big|_{s = -m_{i,r} \lambda_{i,r}}$. Whereas, for PU network, the PR suffers from two interfering signals caused by S and EA of R. The CDF of the channel matrix $\mathbf{c}_{s,pr}$ between S and PR is similar to (7), when replacing $m_{s,j}$ and $\lambda_{s,j}$ by $m_{s,pr}$ and $\lambda_{s,pr}$, respectively. While, the CDF of channel $c_{r,pr}$ follows i.i.d. Nakagami-m fading model, which is given by

$$F_{|c_{r,pr}|^2}(z) = 1 - \sum_{k=0}^{m_{r,pr} - 1} \frac{\left(m_{r,pr} \lambda_{r,pr} z \right)^k}{k!} \exp\left(-m_{r,pr} \lambda_{r,pr} z \right), \tag{10}$$

where $\lambda_{r,pr} = 1/\bar{\gamma}_{r,pr}$, $\bar{\gamma}_{r,pr} = \frac{P_r}{\sigma_{pr}^2} \mathbb{E}\{|h_{r,pr}|^2\} = \frac{P_r}{\sigma_{pr}^2} \Omega_{r,pr}$, and $m_{r,pr}$ denotes the Nakagami-m fading parameter between R and PR. Hence, the pdf is obtained by differentiating (10) w.r.t. z as follows

$$f_{|c_{r,pr}|^2}(z) = \frac{\left(m_{r,pr} \lambda_{r,pr} \right)^{m_{r,pr}} z^{m_{r,pr} - 1}}{\Gamma(m_{r,pr})} \exp(-m_{r,pr} \lambda_{r,pr} z). \tag{11}$$

2.2.3 For Data Transmission Over FSO Link: The FSO link between R and D experiences a Málaga-$\mathcal{M}$ fading model with the effect of pointing errors. The $\mathcal{M}$ turbulence model [37] is based on a physical model that involves a line-of-sight (LOS) contribution, U_L, a component that is quasi-forward scattered by the eddies on the propagation axis and coupled to the LOS contribution, U_S^C, and another component, U_S^G, due to energy that is scattered to the receiver by off-axis eddies. These random processes, U_S^C and U_S^G are statistically independent. Additionally, the random processes,

U_L and U_S^G are statistically independent. One of the main motivations to consider this model is its generality [37, Table 1]. Hence, we employ a FSO link that experiences $\mathcal{M}$ turbulence for which the SNR's CDF is given by [8]

$$F_{\widetilde{\gamma}_{s,r}}(\gamma) = D \sum_{v=1}^{\beta} C_v \mathrm{G}_{r+1,3r+1}^{3r,1}\left[\frac{E}{\mu_r}\gamma \middle| \begin{matrix} 1, \chi_1 \\ \chi_2, 0 \end{matrix}\right], \tag{12}$$

where $D = \zeta^2 A / [2^r (2\pi)^{r-1}]$, ζ is the ratio between the equivalent beam radius at the receiver and the pointing error displacement standard deviation at the receiver, $A = \frac{2\alpha^{\frac{\alpha}{2}}}{g^{1+\frac{\alpha}{2}}\Gamma(\alpha)}(\frac{g\beta}{g\beta+\Omega'})^{\beta+\frac{\alpha}{2}}$, with α is a positive parameter related to the effective number of large-scale cells of the scattering process, β is the amount of fading parameter and is a natural number, $g = \mathbb{E}\left[|U_S^G|^2\right] = 2b_0(1-\rho)$ denotes the average power of the scattering component received by off-axis eddies, $2b_0 = \mathbb{E}\left[|U_S^C|^2 + |U_S^G|^2\right]$ is the average power of the total scatter components, the parameter $0 \leq \rho \leq 1$ represents the amount of scattering power coupled to the LOS component, $\Omega' = \Omega + 2b_0\rho + 2\sqrt{2b_0\rho\Omega}\cos(\phi_A - \phi_B)$ represents the average power from the coherent contributions, $\Omega = \mathbb{E}\left[|U_L|^2\right]$ is the average power of the LOS component, ϕ_A and ϕ_B are the deterministic phases of the LOS and the coupled-to-LOS scatter terms, respectively, and $\Gamma(.)$ is the Gamma function as defined in [34, Eq. (8.310)]. It is interesting to know here that $\mathbb{E}\left[|U_S^C|^2\right] = 2b_0\rho$ denotes the average power of the coupled-to-LOS scattering component, r is the parameter defining the type of detection technique (i.e. $r = 1$ for heterodyne detection, and $r = 2$ for intensity modulation (IM)/direct detection (DD)), $C_v = B_v r^{\alpha+v-1}$, with $B_v = A_v[\alpha\beta/(g\beta+\Omega')]^{-(\alpha+v)/2}$, with $A_v = \binom{\beta-1}{v-1}\frac{(g\beta+\Omega')^{1-v/2}}{(v-1)!}\left(\frac{\Omega'}{g}\right)^{v-1}\left(\frac{\alpha}{\beta}\right)^{v/2}$, $\mathrm{G}[.]$ is the Meijer G-function as defined in [34, Eq. (9.301)], $E = B^r/r^{2r}$, with $B = \zeta^2\alpha\beta(g+\Omega')/[(\zeta^2+1)(g\beta+\Omega')]$, for μ_r, when $r = 1$, $\mu_1 = \mu_{\text{heterodyne}}$ and when $r = 2$, $\mu_2 = \mu_{\text{IM/DD}}$, $\chi_1 = \frac{\zeta^2+1}{r}, \ldots, \frac{\zeta^2+r}{r}$ comprises of r terms, and $\chi_2 = \frac{\zeta^2}{r}, \ldots, \frac{\zeta^2+r-1}{r}, \frac{\alpha}{r}, \ldots, \frac{\alpha+r-1}{r}, \frac{v}{r}, \ldots, \frac{v+r-1}{r}$ comprises of $3r$ terms.

2.2.4 For Energy Transmission: The entries $h_{q,i}$, with $q \in \{pt, r\}$ and $i = 1, 2, \ldots, N_s$ of the channel vector $\mathbf{h}_{q,s}$ represent the channel coefficients between the energy transmitters and the i-th antenna of the SU source S. These coefficients follow i.i.d. Nakagami-m fading model. Hence, the CDF of $\mathbf{h}_{q,s}$ assuming MRC at S is given by (7), but with replacing $m_{s,j}$ and $\lambda_{s,j}$ by their counterparts $m_{q,s}$ and $\lambda_{q,s}$, respectively.

3. Performance Analysis

Closed-form expressions for the system outage probability, average BER, and ergodic capacity are derived in this section. Then, at the high SNR regime, the asymptotic formulas are obtained.

3.1 Outage Probability

3.1.1 Exact Outage Probability: For the proposed EH-CRN, the outage probability is defined as the probability that $\gamma_{s,d}$ value is below a predetermined outage threshold γ_{th} such as $P_{out}(\gamma_{out}) = \Pr[\gamma_{s,d} \leq \gamma_{th}] = \Pr[\min\{\gamma_{\text{RF}}, \gamma_{\text{FSO}}\} \leq \gamma_{th}]$. Based on (6), the CDF of $\gamma_{s,d}$ can be written as

$$F_{\gamma_{s,d}}(\gamma) = F_{\gamma_{\text{RF}}}(\gamma) + F_{\gamma_{\text{FSO}}}(\gamma) - F_{\gamma_{\text{RF}}}(\gamma)F_{\gamma_{\text{FSO}}}(\gamma), \tag{13}$$

where $F_{\gamma_{\text{RF}}}(\gamma)$ is the CDF of SINR of the RF link, and $F_{\gamma_{\text{FSO}}}(\gamma)$ is the CDF of SNR of the FSO link. For the RF link, the SU network will be in outage if one or more of three events occurs. These three events can be specified as follows: The first outage event occurs if the SU total interference signals for data and energy transmissions at the primary network exceed the PU maximum interference threshold γ_P. The second outage event occurs if the SU SINR at R is less than γ_{th}, and hence, R can not decode the SU data correctly. Finally, the third outage event occurs if the total harvesting energy received by S is less than the energy harvesting threshold γ_E. Therefore, the SU network outage probability can be expressed as the complementary probability that all of the above-mentioned

events do not happen, such as

$$F_{\gamma_{\mathrm{RF}}}(\gamma) = 1 - \Pr\left[\frac{P_s}{N_s}\left\|\mathbf{c}_{s,pr}\right\|^2 + P_e\left|c_{r,pr}\right|^2 \le \gamma_P\right]\Pr\left[\gamma_{\mathrm{RF}} \ge \gamma_{th}\right]\Pr\left[P_{pt}\left\|\mathbf{h}_{pt,s}\right\|^2 + P_e\left\|\mathbf{h}_{r,s}\right\|^2 \ge \gamma_E\right]. \tag{14}$$

The analysis for obtaining the expression of the terms $\Pr[\frac{P_s}{N_s}\|\mathbf{c}_{s,pr}\|^2 + P_e|c_{r,pr}|^2 \le \gamma_P]$, $\Pr[\gamma_{\mathrm{RF}} \ge \gamma_{th}]$, and $\Pr[P_{pt}\|\mathbf{h}_{pt,s}\|^2 + P_e\|\mathbf{h}_{r,s}\|^2 \ge \gamma_E]$ are given, respectively by

$$\begin{aligned}
&\Pr\left[\frac{P_s}{N_s}\left\|\mathbf{c}_{s,pr}\right\|^2 + P_e\left|c_{r,pr}\right|^2 \le \gamma_P\right] = 1 - \int_0^\infty F_{\|\mathbf{h}_{s,r}\|^2}((x+1)\gamma_{th}) f_{\sum_{i\in\{pt,r\}}|c_{i,r}|^2}(x)dx \\
&= 1 - \sum_{q=0}^{m_{e,r}-1}\frac{(m_{e,r}\lambda_{e,r}\gamma_P)^q}{q!}\exp(-m_{e,r}\lambda_{e,r}\gamma_P) - \sum_{u=0}^{m_{s,r}N_s-1}\frac{(m_{s,r}\lambda_{s,r})^u}{\Gamma(m_{e,r}+u+1)}(m_{e,r}\lambda_{e,r})^{m_{e,r}} \\
&\quad\times \exp(-m_{e,r}\lambda_{s,r}\gamma_P)\gamma_P^{u+m_{e,r}}{}_1F_1\left(m_{e,r}, p+m_{e,r}+1, (m_{s,r}\lambda_{s,r}-m_{e,r}\lambda_{e,r})\gamma_p\right),
\end{aligned} \tag{15}$$

$$\begin{aligned}
&\Pr\left[\gamma_{\mathrm{RF}} \ge \gamma_{th}\right] = 1 - \Pr\left[\gamma_{\mathrm{RF}} < \gamma_{th}\right] = 1 - \int_0^\infty F_{\|\mathbf{h}_{s,r}\|^2}((x+1)\gamma_{th}) f_{\sum_{i\in\{pt,r\}}|c_{i,r}|^2}(x)dx \\
&= \left[\prod_{i\in\{pt,r\}}(m_{i,r}\lambda_{i,r})^{m_{i,r}}\right]\sum_{i\in\{pt,r\}}\sum_{j=1}^{m_{i,r}}\sum_{k=0}^{m_{s,r}N_s-1}\frac{\beta_{i,r}^{j-1}(m_{s,r}\lambda_{s,r}\gamma_{\mathrm{th}})^k}{(j-1)!k!}\exp(-m_{s,r}\lambda_{s,r}\gamma_{th}) \\
&\quad\times U(m_{i,r}-j+1, m_{i,r}+k-j+2, m_{i,r}\lambda_i + m_{s,r}\lambda_{s,r}\gamma_{th}),
\end{aligned} \tag{16}$$

$$\begin{aligned}
&\Pr\left[P_{pt}\left\|\mathbf{h}_{pt,s}\right\|^2 + P_e\left\|\mathbf{h}_{r,s}\right\|^2 \ge \gamma_E\right] = 1 - \int_0^{\gamma_E} F_{\|\mathbf{h}_{pt,s}\|^2}(\gamma_E - x) f_{\|\mathbf{h}_{r,s}\|^2}(x) \\
&= \sum_{p=0}^{m_{pt,s}N_s-1}\frac{(m_{pt,s}\lambda_{pt,s}\gamma_E)^p}{p!}\exp(-m_{pt,s}\lambda_{pt,s}\gamma_E) + \sum_{q=0}^{m_{e,s}N_s-1}(m_{e,s}\lambda_{e,s})^q\frac{(m_{pt,s}\lambda_{pt,s})^{m_{pt,s}N_s}\exp(-m_{e,s}\lambda_{e,s}\gamma_E)}{\Gamma(m_{pt,s}N_s+q+1)\gamma_E^{-m_{pt,s}N_s-q}} \\
&\quad\times {}_1F_1\left(m_{pt,s}N_s, m_{pt,s}N_s+q+1, (m_{e,s}\lambda_{e,s}-m_{e,s}\lambda_{pt,s})\gamma_E\right).
\end{aligned} \tag{17}$$

On the other hand, the CDF $F_{\gamma_{\mathrm{FSO}}}(\gamma)$ is given by (12). By substituting (12) and (14) in (13) and replacing γ by γ_{th}, the system outage probability is given by

$$\begin{aligned}
P_{out}(\gamma_{th}) = &\left\{1 - \Pr\left[\frac{P_s}{N_s}\left\|\mathbf{c}_{s,pr}\right\|^2 + P_e\left|c_{r,pr}\right|^2 \le \gamma_P\right]\Pr\left[\gamma_{\mathrm{RF}} \ge \gamma_{th}\right]\Pr\left[P_{pt}\left\|\mathbf{h}_{pt,s}\right\|^2 + P_e\left\|\mathbf{h}_{r,s}\right\|^2 \ge \gamma_E\right]\right\} \\
&\times\left\{1 - D\sum_{v=1}^{\beta}C_v\mathrm{G}_{r+1,3r+1}^{3r,r}\left[E\frac{\gamma_{th}}{\mu_r}\middle|\begin{matrix}1,\kappa_1\\ \kappa_2,0\end{matrix}\right]\right\} + D\sum_{v=1}^{\beta}C_v\mathrm{G}_{r+1,3r+1}^{3r,r}\left[E\frac{\gamma_{th}}{\mu_r}\middle|\begin{matrix}1,\kappa_1\\ \kappa_2,0\end{matrix}\right].
\end{aligned} \tag{18}$$

3.1.2 Asymptotic Outage Probability: A simple asymptotic expression for the outage probability is derived which achieves more insights about the system behavior. At high SNR values, the outage probability can be expressed as $P_{out} \simeq (G_c\mathrm{SNR})^{-G_d}$, where G_c denotes the coding gain of the system and G_d is the diversity order of the RF link [38]. Hence, as $\gamma_{\mathrm{RF}} \to \infty$, the CDF of the RF link's SNR at R is simplified to

$$F_{\gamma_{\mathrm{RF}}}^{\infty}(\gamma) = 1 - \Pr\left[\frac{P_s}{N_s}\left\|\mathbf{c}_{s,pr}\right\|^2 + P_e\left|c_{r,pr}\right|^2 \le \gamma_P\right]\overset{\infty}{\Pr}\left[\gamma_{\mathrm{RF}} \ge \gamma_{th}\right]\Pr\left[P_{pt}\left\|\mathbf{h}_{pt,s}\right\|^2 + P_e\left\|\mathbf{h}_{r,s}\right\|^2 \ge \gamma_E\right], \tag{19}$$

where $\Pr^{\infty}[\gamma_{\mathrm{RF}} \geq \gamma_{th}]$ is the asymptotic probability at SNR $\rightarrow \infty$ such as

$$\overset{\infty}{\Pr}[\gamma_{\mathrm{RF}} \geq \gamma_{th}] = 1 - \prod_{i\in\{pt,r\}} (m_{i,r}\lambda_{i,r})^{m_{i,r}} \sum_{i\in\{pt,r\}} \sum_{j=1}^{m_{i,r}} \frac{\beta_{i,r}^{j-1} (m_{s,r}\lambda_{s,r}\gamma_{th})^{m_{s,r}N_s}}{(j-1)!\,(m_{s,r}N_s)!} \times U\left(m_{i,r}-j+1, m_{i,r}+m_{s,r}N_s-j+2, m_{i,r}\lambda_{i,r}\right). \tag{20}$$

For the FSO link, the asymptotic CDF for the Málaga-$\mathcal{M}$ turbulence model is given by [8]

$$F_{\gamma_{\mathrm{FSO}}}^{\infty}(\gamma) \approx D \sum_{v=1}^{\beta} C_v \sum_{k=1}^{3r} \left(\frac{\mu_r}{E\gamma}\right)^{\kappa_{2,k}} \frac{\prod_{l=1;l\neq k}^{3r} \Gamma(\kappa_{2,l}-\kappa_{2,k})}{\kappa_{2,k}\prod_{l=2}^{r+1}\Gamma(\kappa_{1,l}-\kappa_{2,k})}, \tag{21}$$

where $\kappa_{i,j}$ denotes the j-th term of κ_i. Hence, the FSO asymptotic performance is dominated by the $\min(\xi^2, \alpha, \beta)$ as shown in [8]. Therefore, the asymptotic outage probability can be written as

$$P_{out}^{\infty} = 1 - \Pr\left[\frac{P_s}{N_s}\left\|\mathbf{c}_{s,pr}\right\|^2 + P_e\left|c_{r,pr}\right|^2 \leq \gamma_P\right] \overset{\infty}{\Pr}[\gamma_{\mathrm{RF}} \geq \gamma_{th}] \Pr\left[P_{pt}\left\|\mathbf{h}_{pt,s}\right\|^2 + P_e\left\|\mathbf{h}_{r,s}\right\|^2 \geq \gamma_E\right] + D\sum_{v=1}^{\beta} C_v \sum_{k=1}^{3r}\left(\frac{\mu_r}{E\gamma_{out}}\right)^{\kappa_{2,k}} \frac{\prod_{l=1;l\neq k}^{3r}\Gamma(\kappa_{2,l}-\kappa_{2,k})}{\kappa_{2,k}\prod_{l=2}^{r+1}\Gamma(\kappa_{1,l}-\kappa_{2,k})}. \tag{22}$$

As a result, the diversity gain of the proposed system model is of order $\min(m_{sr}N_s, \xi^2/r, \alpha/r, \beta/r)$.

3.2 Average Bit Error Rate

3.2.1 Exact Average Bit Error Rate: For the considered system, the average BER can be obtained using the following formula [39]

$$P_{\mathrm{BER}} = P_{\mathrm{BER}}^{\mathrm{RF}} + P_{\mathrm{BER}}^{\mathrm{FSO}} - 2P_{\mathrm{BER}}^{\mathrm{RF}}P_{\mathrm{BER}}^{\mathrm{FSO}}, \tag{23}$$

where $P_{\mathrm{BER}}^{\mathrm{RF}}$ and $P_{\mathrm{BER}}^{\mathrm{FSO}}$ are the average BERs for the first and second hop, respectively. These average BERs can be obtained using the obtained CDF expressions as follows

$$P_{\mathrm{BER}}^{\mathrm{RF}} = \frac{a_{rf}\sqrt{b_{rf}}}{2\sqrt{\pi}} \int_0^{\infty} \frac{\exp(-b_{rf}\gamma)}{\sqrt{\gamma}} F_{\gamma_{\mathrm{RF}}}(\gamma)\, d\gamma, \tag{24}$$

$$P_{\mathrm{BER}}^{\mathrm{FSO}} = \frac{a_{fso}\sqrt{b_{fso}}}{2\sqrt{\pi}} \int_0^{\infty} \frac{\exp(-b_{fso}\gamma)}{\sqrt{\gamma}} F_{\gamma_{\mathrm{FSO}}}(\gamma)\, d\gamma, \tag{25}$$

where a_{rf}, b_{rf}, a_{fso}, and b_{fso} denote the modulation type used in both RF and FSO links, respectively. Hence, by substituting (14) in (24), the average BER of RF link is given by

$$P_{\mathrm{BER}}^{\mathrm{RF}} = \frac{a_{rf}}{2} - \frac{a_{rf}\sqrt{b_{rf}}}{2\sqrt{\pi}} \Pr\left[\frac{P_s}{N_s}\left\|\mathbf{c}_{s,pr}\right\|^2 + P_e\left|c_{r,pr}\right|^2 \leq \gamma_P\right] \Pr\left[P_{pt}\left\|\mathbf{h}_{pt,s}\right\|^2 + P_e\left\|\mathbf{h}_{r,s}\right\|^2 \geq \gamma_E\right] \times \prod_{i\in\{pt,r\}} (m_{i,r}\lambda_{i,r})^{m_{i,r}} \sum_{i\in\{pt,r\}} \sum_{j=1}^{m_{i,r}} \frac{\beta_{i,r}^{j-1}}{(j-1)!} \sum_{k=0}^{m_{s,r}N_s-1} \frac{(m_{s,r}\lambda_{s,r})^k}{k!} \sum_{q=0}^{k} \binom{k}{k-q} \frac{(m_{i,r}+q-j)!\Gamma\left(\frac{m_{i,r}\lambda_{i,r}}{m_{s,r}\lambda_{s,r}}\right)}{(m_{i,r}-j)!\left(b_{rf}+m_{s,r}\lambda_{s,r}\right)} \times \frac{(m_{s,r}\lambda_{s,r})^{-(m_{i,r}+q-j+1)}}{\left(\frac{m_{i,r}\lambda_{i,r}}{m_{s,r}\lambda_{s,r}}\right)^{\frac{m_{i,r}+q-k-j+3/2}{2}}} U\left(m_{i,r}+q-j+1, m_{i,r}+q-k-j+\frac{3}{2}, \left(b_{rf}+m_{s,r}\lambda_{s,r}\right)\frac{m_{i,r}\lambda_{i,r}}{m_{s,r}\lambda_{s,r}}\right). \tag{26}$$

Similarly, by substituting (12) in (25) with the help of [8], the BER of the FSO link is given by

$$P_{\mathrm{BER}}^{\mathrm{FSO}} = \frac{a_{fso} D}{2\sqrt{\pi}} \sum_{v=1}^{\beta} C_v \mathrm{G}_{r+2,3r+1}^{3r,2} \left[\frac{E}{b_{fso}\mu_r} \middle| \begin{matrix} 0.5, 1, \kappa_1 \\ \kappa_2, 0 \end{matrix} \right]. \tag{27}$$

Finally, the expression for the exact average BER is obtained by substituting (26) and (27) in (23).

3.2.2 Asymptotic Average Bit Error Rate: To get more insights on the key system parameters affecting the system performance, a closed-form expression for the system asymptotic average BER is derived such as

$$P_{\mathrm{BER}}^{\infty} \approx P_{\mathrm{BER}}^{\mathrm{RF},\infty} + P_{\mathrm{BER}}^{\mathrm{FSO},\infty}, \tag{28}$$

where $P_{\mathrm{BER}}^{\mathrm{RF},\infty}$ and $P_{\mathrm{BER}}^{\mathrm{FSO},\infty}$ are the asymptotic BERs of both RF and FSO links, respectively. By substituting (19) in (24), the asymptotic average BER of the RF link is given by

$$P_{\mathrm{BER}}^{\mathrm{RF},\infty} = \frac{a_{rf}}{2} - \Pr\left[\frac{P_s}{N_s} \left\| \mathbf{c}_{s,pr} \right\|^2 + P_e \left| c_{r,pr} \right|^2 \le \gamma_P \right] \Pr\left[P_{pt} \left\| \mathbf{h}_{pt,s} \right\|^2 + P_e \left\| \mathbf{h}_{r,s} \right\|^2 \ge \gamma_E \right] \Bigg\{ \frac{a_{rf}}{2} - \frac{a_{rf}}{2\sqrt{\pi}}$$
$$\times \prod_{i\in\{pt,r\}} (m_{i,r}\lambda_{i,r})^{m_{i,r}} \sum_{i\in\{pt,r\}} \sum_{j=1}^{m_{i,r}} \frac{\beta_{i,r}^{j-1}}{(j-1)!} \frac{(m_{s,r}\lambda_{s,r})^{m_{s,r}N_s} \Gamma\left(m_{s,r}N_s + \frac{1}{2}\right)}{b_{rf}^{m_{s,r}N_s} (m_{s,r}N_s)!}$$
$$\times U\left(m_{i,r} - j + 1, m_{i,r} + m_{s,r}N_s - j + 2, m_{i,r}\lambda_{i,r}\right) \Bigg\}. \tag{29}$$

Similarly, by substituting (12) in (25), the asymptotic average BER of the FSO link is given by

$$P_{\mathrm{BER}}^{\mathrm{FSO},\infty} \approx \frac{a_{fso} D}{2\sqrt{\pi}} \sum_{v=1}^{\beta} C_v \sum_{k=1}^{3r} \left(\frac{b_{fso}\mu_r}{E} \right)^{-\kappa_{2,k}} \frac{\Gamma\left(\kappa_{2,k} + a_{fso}\right) \prod_{l=1;l\neq k}^{3r} \Gamma\left(\kappa_{2,l} - \kappa_{2,k}\right)}{\kappa_{2,k} \prod_{l=3}^{r+2} \Gamma\left(\kappa_{1,l} - \kappa_{2,k}\right)}. \tag{30}$$

3.3 Ergodic Channel Capacity

The ergodic capacity $\mathcal{C}_{\mathrm{erg}}$ for dual-hop mixed RF/FSO networks can be expressed as

$$\mathcal{C}_{\mathrm{erg}} = \frac{1}{2} \min\left\{ \mathbf{E}\left[\mathcal{C}_{\mathrm{RF}}\right], \mathbf{E}\left[\mathcal{C}_{\mathrm{FSO}}\right] \right\}, \tag{31}$$

where $\mathcal{C}_{\mathrm{RF}}$ denotes the RF channel capacity and given by

$$\mathcal{C}_{\mathrm{RF}} = \log\left(1 + \gamma_{\mathrm{RF}}\right) = \frac{1}{\ln(2)} \int_0^{\infty} \frac{1 - F_{\gamma_{\mathrm{RF}}}(\gamma)}{1+\gamma} d\gamma,$$
$$= \frac{1}{\ln(2)} \Pr\left[\frac{P_s}{N_s} \left\| \mathbf{c}_{s,pr} \right\|^2 + P_e \left| c_{r,pr} \right|^2 \le \gamma_P \right] \Pr\left[P_{pt} \left\| \mathbf{h}_{pt,s} \right\|^2 + P_e \left\| \mathbf{h}_{r,s} \right\|^2 \ge \gamma_E \right] \prod_{i\in\{pt,r\}} (m_{i,r}\lambda_{i,r})^{m_{i,r}}$$
$$\times \sum_{i\in\{pt,r\}} \sum_{j=1}^{m_{i,r}} \frac{\beta_{i,r}^{j-1}}{(j-1)!} \sum_{k=0}^{m_{s,r}N_s - 1} \frac{m_{s,r}\lambda_{s,r}}{k!} \exp(m_{i,r}\lambda_{i,r}) \sum_{t=0}^{\infty} \frac{(-m_{i,r}\lambda_{i,r})^t}{t!} G_{4,3}^{1,4} \left[\frac{1}{m_{s,r}\lambda_{s,r}} \middle| \begin{matrix} 1-k, 1, t-k+1, t+m_{i,r}-j+2 \\ 1, t+1, t-k+1 \end{matrix} \right]. \tag{32}$$

Whereas, $\mathcal{C}_{\mathrm{FSO}}$ is the FSO channel capacity such as

$$\mathcal{C}_{\mathrm{FSO}} == \frac{1}{\ln(2)} \int_0^{\infty} \frac{1 - F_{\gamma_{\mathrm{FSO}}}(\nu_r \gamma)}{1 + \nu_r \gamma} d\gamma = \frac{D}{\ln(2)} \sum_{v=1}^{\beta} C_v \mathrm{G}_{r+2,3r+2}^{3r+2,1} \left[\frac{E}{\nu_r \mu_r} \middle| \begin{matrix} 0, 1, \kappa_1 \\ \kappa_2, 0, 0 \end{matrix} \right], \tag{33}$$

where ν_r with $r \in \{1, 2\}$ is a constant such that $\nu_1 = 1$ for heterodyne detection and $\nu_2 = \sqrt{e/2\pi}$ for IM/DD detection [8].

4. Proposed Power Optimization Model

4.1 Simplified Asymptotic Outage Probability

In this part, a more simplified asymptotic outage probability expression is derived. Consider that the PU interference threshold is large enough such as $\gamma_P >> \frac{P_s}{N_s}\left\|\mathbf{c}_{s,pr}\right\|^2 + P_e\left|c_{r,pr}\right|^2$. Therefore, the asymptotic outage probability can be simplified further as follows

$$\widehat{P}_{\text{out}}^{\infty} = 1 - \overset{\infty}{\Pr}[\gamma_{\text{RF}} \geq \gamma_{th}]\overset{\infty}{\Pr}\left[P_{pt}\left\|\mathbf{h}_{pt,s}\right\|^2 + P_e\left\|\mathbf{h}_{r,s}\right\|^2 \geq \gamma_E\right]. \tag{34}$$

It is clear that the term $\Pr\left[\frac{P_s}{N_s}\left\|\mathbf{c}_{s,pr}\right\|^2 + P_e\left|c_{r,pr}\right|^2 \leq \gamma_P\right]$ can be ignored assuming that γ_P is large enough. The term $\Pr^{\infty}[\gamma_{\text{RF}} \geq \gamma_{th}]$ is given by (20). Assuming high SNR regime, $P_e \to \infty$, hence, $\lambda_{r,r} \to 0$, then, $\Pr^{\infty}[\gamma_{\text{RF}} \geq \gamma_{th}]$ can be re-expressed as

$$\overset{\infty}{\Pr}[\gamma_{\text{RF}} \geq \gamma_{th}] = 1 - \frac{\Psi}{\lambda_{s,r}^{-m_{s,r}N_s}}\left(\sum_{j=1}^{m_{pt,r}}\sum_{q=0}^{m_{pt,r}-j+1}\frac{\Upsilon_{j,q}^{td}}{\lambda_{r,r}^{-(m_{pt,r}+m_{r,r}-j+1-q)}} + \sum_{i=1}^{m_{r,r}}\sum_{p=0}^{m_{r,r}-i+1}\frac{\Upsilon_{i,p}^{ed}}{\lambda_{r,r}^{-(i-1+p)}}\right), \tag{35}$$

where $\Psi = (m_{pt,r}\lambda_{pt,r})^{m_{pt,r}}\frac{(m_{s,r}\gamma_{\text{th}})^{m_{s,r}N_s}}{(m_{s,r}N_s)!}$, $\Upsilon_{j,q}^{td} = \frac{(m_{pt,r})!(-1)^q(m_{pt,r}\lambda_{pt,r})^q}{(m_{pt,r}-j+1)(j-1)!}\binom{m_{pt,r}-j+1}{q}m_{r,r}^{m_{pt,r}+m_{r,r}-j+1-q}U(m_{pt,r}-j+1, m_{pt,r}+m_{s,r}N_s-j+2, m_{pt,r}\lambda_{pt,r})$, and $\Upsilon_{i,p}^{ed} = \frac{(m_{r,r})!(-1)^p}{(m_{r,r}-i+1)(i-1)!}\binom{m_{r,r}-i+1}{p}(m_{r,r})^{i-1+p}(\lambda_{pt,r}m_{pt,r})^{m_{r,r}-i+1-p}$. Whereas, the term $\Pr^{\infty}[P_{pt}\left\|\mathbf{h}_{pt,s}\right\|^2 + P_e\left\|\mathbf{h}_{r,s}\right\|^2 \geq \gamma_E]$ can be obtained as follows

$$\overset{\infty}{\Pr}\left[P_{pt}\left\|\mathbf{h}_{pt,s}\right\|^2 + P_e\left\|\mathbf{h}_{r,s}\right\|^2 \geq \gamma_E\right] = 1 - \int_0^{\gamma_E} F_{\text{MA}}^{\infty}(\gamma_E - x)f_{\text{MA}}(x)dx = 1 - \Xi \times \left(\frac{\sigma_0^2}{\Omega_{r,s}P_e}\right)^{m_{r,s}N_s}, \tag{36}$$

where $\Xi = \frac{(m_{r,s})^{m_{r,s}N_s}(m_{pt,s}\lambda_{pt,s})^{m_{pt,s}N_s}}{(m_{r,s}N_s+m_{pt,s}N_s)!\gamma_E^{-(m_{pt,s}+m_{r,s})N_s}}{}_1F_1\left(m_{pt,s}N_s, (m_{pt,s}+m_{r,s})N_s+1, -m_{pt,s}\lambda_{pt,s}\gamma_E\right)$.

4.2 Power Optimization Problem

This part aims to find the optimal P_e that minimizes the outage probability. For simplicity and without loss of generality, the simplified asymptotic outage probability expression in (34) is used as a target function to formulate the power optimization problem as follows

$$\min_{P_e}\widehat{P}_{\text{out}}(P_e), \qquad \text{subject to} \begin{cases} \frac{P_{\text{sen}}-\Omega_{pt,s}P_T}{\Omega_{r,s}} \leq P_e \\ P_e > 0 \end{cases}, \tag{37}$$

where $\widehat{P}_{\text{out}}^{\infty}$ is given in (34). By substituting (35) and (36) in (34), the total P_{out}^{∞} can be expressed in terms of P_e with some mathematical manipulations as follows

$$\widehat{P}_{\text{out}}^{\infty} = \widetilde{\Psi}\left[\sum_{j=1}^{m_{pt,r}}\sum_{q=0}^{m_{pt,r}-j+1}\frac{\widetilde{\Upsilon}_{j,q}^{td}}{P_e^{m_{pt,r}+m_{r,r}-j+1-q}} + \sum_{i=1}^{m_{r,r}}\sum_{p=0}^{m_{r,r}-i+1}\frac{\widetilde{\Upsilon}_{i,p}^{ed}}{P_e^{i-1+p}}\right] + \frac{\widetilde{\Xi}}{P_e^{m_{r,s}N_s}}, \tag{38}$$

where $\widetilde{\Psi} = \frac{\Psi}{P_s^{m_{s,r}N_s}} \times \left(\frac{\sigma_0^2}{\Omega_{s,r}}\right)^{m_{s,r}N_s}$, $\widetilde{\Upsilon}_{j,q}^{td} = \Upsilon_{j,q}^{td} \times \left(\frac{\sigma_0^2}{\Omega_{r,r}}\right)^{m_{pt,r}+m_{r,r}-j+1-q}$, $\widetilde{\Upsilon}_{i,p}^{ed} = \Upsilon_{i,p}^{ed} \times \left(\frac{\sigma_0^2}{\Omega_{r,r}}\right)^{i-1+p}$, and $\widetilde{\Xi} = \Xi \times \left(\frac{\sigma_0^2}{\Omega_{r,r}}\right)^{m_{r,s}N_s}$. By applying the Lagrangian multipliers method such as

$$\mathcal{L}(P_e, \lambda_1) = \widetilde{\Psi}\left[\sum_{j=1}^{m_{pt,r}}\sum_{q=0}^{m_{pt,r}-j+1}\frac{\widetilde{\Upsilon}_{j,q}^{td}}{P_e^{m_{pt,r}+m_{r,r}-j+1-q}} + \sum_{i=1}^{m_{r,r}}\sum_{p=0}^{m_{r,r}-i+1}\frac{\widetilde{\Upsilon}_{i,p}^{ed}}{P_e^{i-1+p}}\right] + \frac{\widetilde{\Xi}}{P_e^{m_{r,s}N_s}}$$
$$+ \lambda_1 \times \left(P_e - \frac{P_{\text{sen}}}{\Omega_{r,s}} + \frac{\Omega_{ts}P_T}{\Omega_{r,s}}\right), \tag{39}$$

where $\mathcal{L}(P_e, \lambda_1)$ denotes the Lagrangian multipliers objective function, whereas λ_1 denotes the Lagrangian multiplier coefficient. By applying KKT conditions and without loss of generality, assume

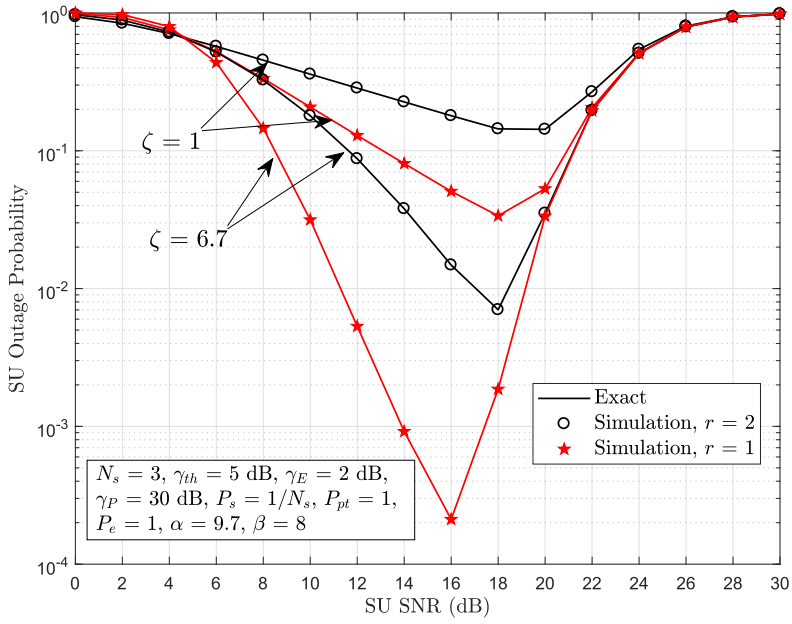

Fig. 2. SU outage probability versus SU SNR for different values of ζ and r.

the SU source is equipped with sufficient number of antennas N_s such that $m_{r,s}N_s > m_{r,r} + m_{pt,r}$, we obtain the following

$$\frac{\partial \mathcal{L}}{\partial P_e} = \sum_{j=1}^{m_{pt,r}} \sum_{q=0}^{m_{pt,r}-j} \widetilde{\Upsilon}_{j,q}^{td} P_e^{m_{r,s}N_s - m_{pt,r} - m_{r,r} + j + q - 1} + \sum_{i=1}^{m_{r,r}} \sum_{p=1}^{m_{r,r}-i+1} \widetilde{\Upsilon}_{i,p}^{ed} P_e^{m_{r,s}N_s - i - p + 1} + \frac{\widetilde{\Xi}}{\widetilde{\Psi}} + \frac{\lambda_1 P_e^{m_{r,s}N_s - 1}}{\widetilde{\Psi}} = 0, \tag{40}$$

$$\frac{\partial \mathcal{L}}{\partial \lambda_1} = P_e - \frac{P_{\text{sen}} - \Omega_{pt,s} P_T}{\Omega_{r,s}} = 0. \tag{41}$$

It is clear that (40) is a polynomial of degree $m_{r,s}N_s - 1$, therefore, the optimal value P_e^* can be obtained by solving (40), and (41) by using any convenient mathematical tool.

5. Simulation and Numerical Results

In this section, some numerical results, which were obtained by using the above-derived expressions are presented together with Monte-Carlo simulation with 10^5 simulations for each SNR value. Several scenarios of various system parameters and their effect on the performance are studied.

The outage probability of the proposed system model is investigated in Figure 2 with different values of ζ for both heterodyne and IM/DD receivers. The results show that increasing ζ enhances the system outage performance. Moreover, the performance of heterodyne receiver (i.e. $r = 1$) outperforms that of the IM/DD receiver (i.e. $r = 2$) as expected. It can be noticed that at low to medium SNR values, the outage performance is enhanced by increasing the SU transmission power. However, at the high SNR values, the proposed system achieves a unity outage probability as the interference of the SU network on the PU network exceeds γ_P, and hence, the SU source reaches a point where it has to terminate its transmission.

To reveal more insights on the key parameters that affect the performance of the proposed system model, we consider $\gamma_P \to \infty$. Figure 3 studies the impact of the Nakagami-m parameter on the system outage probability with $N_s = 2$. The results show that increasing the value of m, enhances the system performance in terms of diversity order. This can be explained as increasing m enhances the performance of the RF link over the FSO link. As a result, the FSO link performance dominates

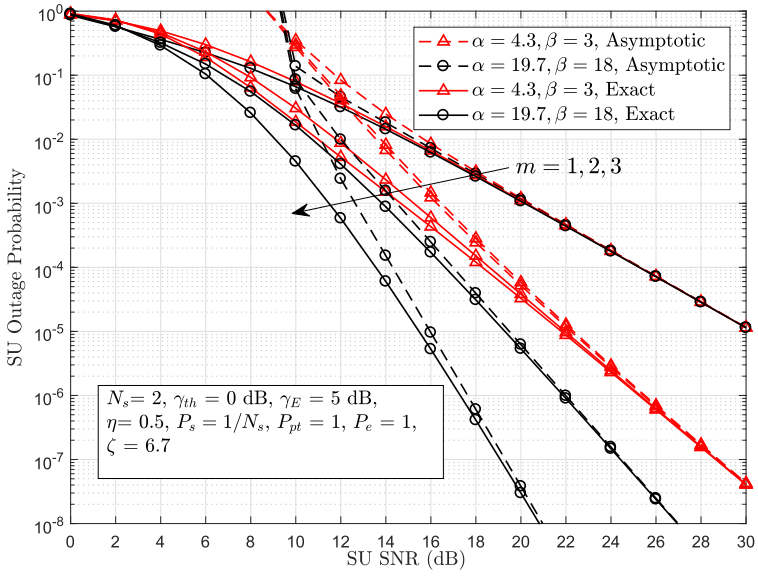

Fig. 3. SU outage probability versus SNR for $\gamma_P \to \infty$ with different values of Nakagami-m parameter, α, and β.

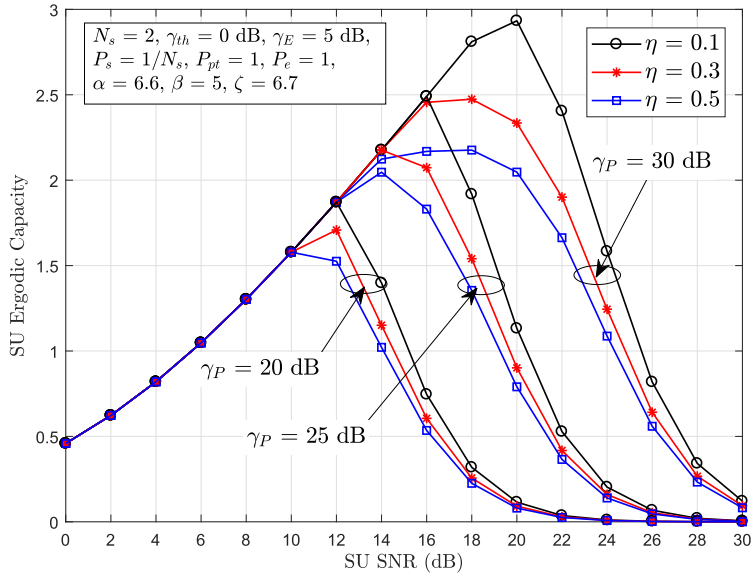

Fig. 4. Ergodic capacity of SU network versus SU SNR for different values of η and γ_P.

the total system performance as the system diversity order is given by min $\left(m_{s,r}N_s, \xi^2/r, \alpha/r, \beta/r\right)$. At weak turbulence conditions (i.e., $\alpha = 19.7$ and $\beta = 18$), the results show that the SU performance is dominated by the RF link, and hence increasing the value of m enhances the system performance in terms of increasing the diversity order. Whereas, at strong turbulence conditions (i.e., $\alpha = 4.3$ and $\beta = 3$), increasing the value of m from 1 to 2 has a significant impact on the system performance. However, as m keeps increasing the SU system performance almost remains constant since the SU performance is dominated by the FSO link.

The SU ergodic capacity is investigated in Figure 4 for different values of η and γ_P. At low SNR values, the results show that increasing the SU SNR increases the capacity for all the values of η and γ_P since the SU system performance is dominated by the FSO link. As the SU SNR

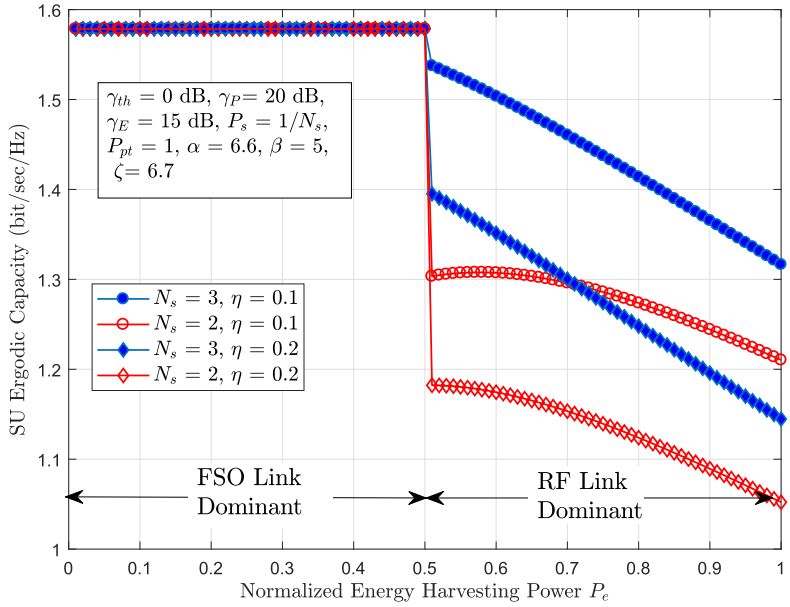

Fig. 5. Ergodic capacity of SU network versus energy harvesting power P_e for different values of η and N_s.

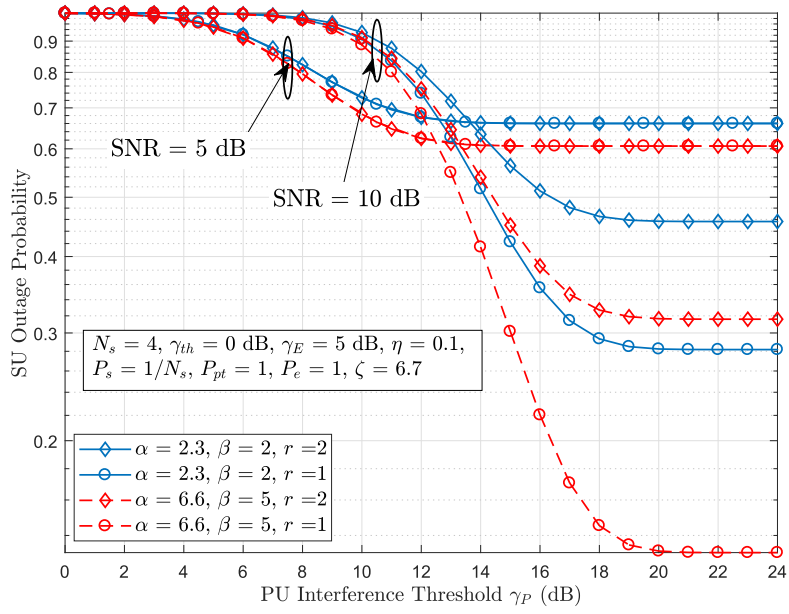

Fig. 6. Outage probability of SU network versus PU interference threshold γ_P for different values of α, β, and r.

keeps increasing, the capacity decreases because the RF dominates the performance, and the SU interference levels at PR go close to γ_P. Then, the capacity drops to zero when the SU interference on the PU network exceeds γ_P causing SU outage. It is clear that increasing γ_P enhances the system capacity as the SU is allowed to transmit at higher power levels. Also, the figure shows that increasing η increases the level of the self-interference at the relay which decreases the system capacity. This degradation becomes significant at higher values of γ_P.

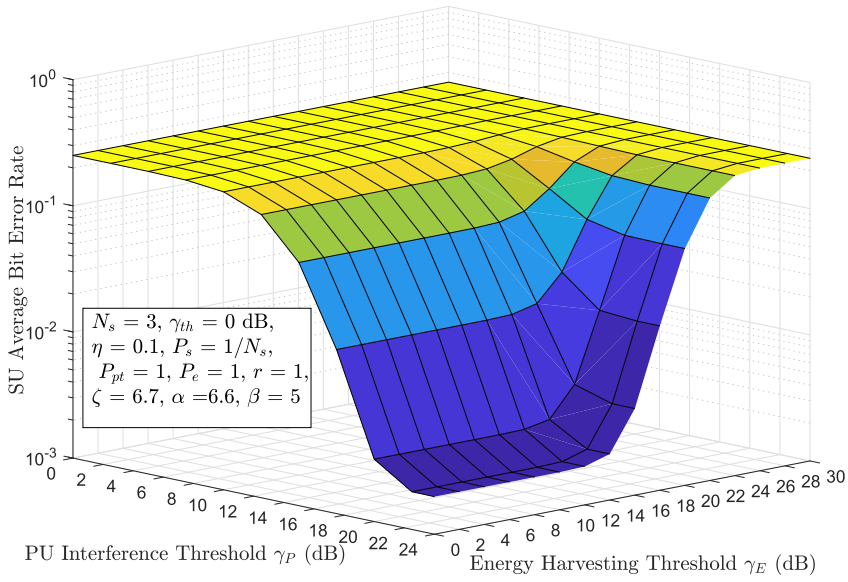

Fig. 7. Average BER of the SU network against OU interference threshold γ_P and energy harvesting threshold γ_E with SNR = 15 dB.

The relation between the ergodic capacity and the harvesting power is studied in Figure 5 for different antenna configurations. It can be noticed that the capacity follows two patterns. In the first pattern, the FSO is the dominant link. Hence, the capacity is not affected by changing the antenna configurations. When the harvested energy goes over the predetermined threshold, the RF link becomes the dominating link and the effect of the antenna configuration starts to take place. As the harvesting power increases, the value of the ergodic capacity decreases. This happens due to the increase in the interference value that leads to decreasing in the SINR and consequently, decreasing the ergodic capacity value.

The effect of PU interference threshold γ_P on the system outage probability is investigated in Figure 6. Apparently, the value of the outage probability decreases as γ_P increases. This can be explained as increasing the threshold gives the SU more chance to pump more transmission power resulting in reducing the outage probability. Moreover, it can be shown that increasing the SNR values from 5 dB to 10 dB reduces the system performance at low to medium γ_P values, whereas, at high γ_P values, the performance of SNR = 10 dB outperforms that of SNR = 5 dB. This can be explained as at low γ_P values; the SU system has to reduce its power to guarantee that its transmission will not harm the PU network. On the other hand, when the PU network relaxes its interference threshold and allows the SU network to transmit with a higher power, the SU performance gets enhanced. Moreover, this figure shows that at low SNR values (i.e., SNR = 5 dB), the performance of the heterodyne receiver matches that of the IM/DD receiver since the performance is dominated by the RF link. At higher SNR values, the performance is dominated by the FSO link. Hence, changing the receiver method has a great impact on the outage performance.

The impact of both γ_E and γ_P on the system average BER performance is shown in Figure 7. For a fixed value of γ_P, the results show that increasing γ_E reduces the system performance as the SU transmitter needs to harvest more power for transmission. On the other hand, the figure shows that for a fixed value of γ_E, increasing γ_P enhances the system performance which matches the results in Figure 6. It is important to mentioned that the modulation schemes are binary phase shift keying (BPSK) ($a_{rf} = b_{rf} = 1$), and on-off keying (OOK) ($a_{fso} = 1$, $b_{fso} = 0.5$) are used in the results of the BER as the modulation schemes for the RF and IM/DD-FSO hops, respectively, while BPSK ($a_{fso} = b_{fso} = 1$) is used for heterodyne receiver-FSO hop.

The impact of atmospheric turbulence conditions on the average BER for different receivers is shown in Figure 8. The results show that the performance of strong turbulence conditions, i.e.

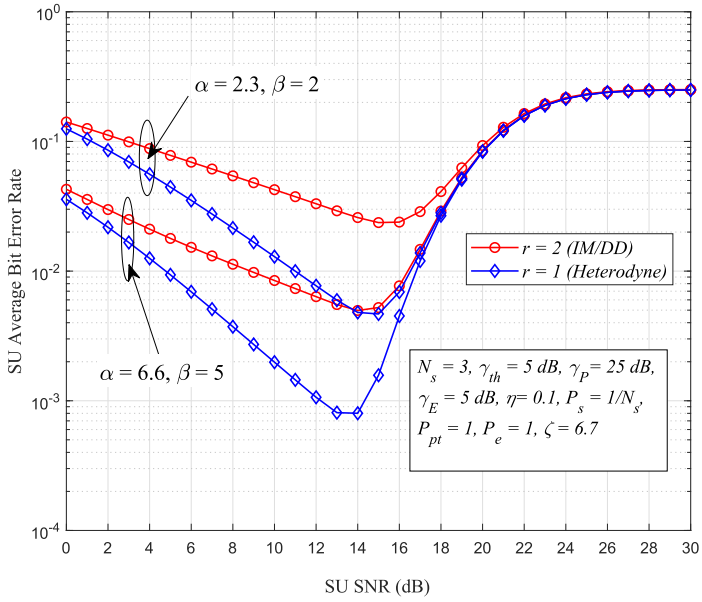

Fig. 8. Average bit error rate of SU network versus SU SNR with different values of α, β, and r.

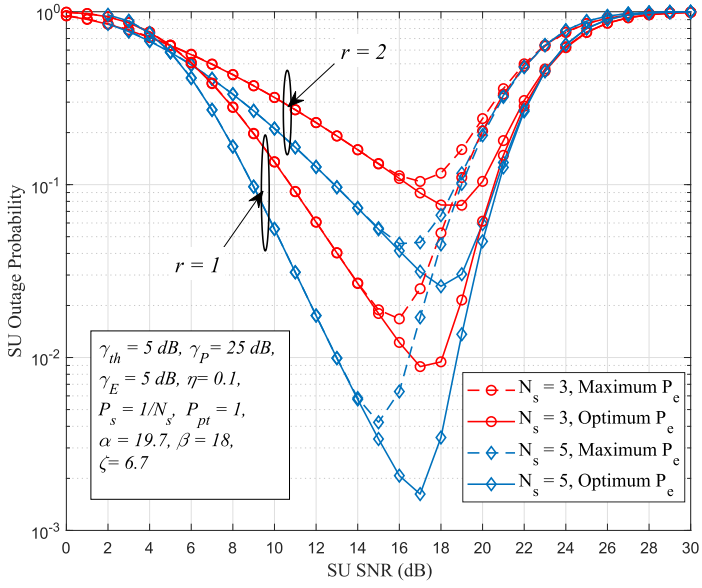

Fig. 9. Outage probability comparison between the proposed optimal P_e value and normalized value with different value of N_s.

$\alpha = 2.3$, $\beta = 2$ is worse than the weak turbulence conditions, i.e. $\alpha = 6.6$, $\beta = 6$ as expected. For high SNR values, the figure shows that the performances of the different turbulence conditions are similar since increasing the SU SNR values causes the outage of SU network. This occurs when the SU interference with the PU is close to γ_P as the RF link dominates the performance.

The impact of the proposed power optimization model on the outage performance is investigated in Figure 9. It is clear that the performance of the proposed power optimization model outperforms that of the conventional transmission model where the energy harvesting antenna transmits with its maximum power, especially, in the medium SNR range. The results show that increasing the number of antennas N_s enhances the performance.

6. Conclusion

This paper investigated the performance of mixed MISO RF/FSO CR relay networks with EH technique. The SU source equipped with multiple antennas communicates with a hybrid relay through a RF channel. Then, the relay forwards the successfully decoded data to the destination over FSO link. Closed-form expressions for the outage probability, average BER, and ergodic capacity were derived assuming Nakagami-m/Málaga-$\mathcal{M}$ fading models with pointing errors on the FSO link. Also, the asymptotic outage probability and average BER were obtained to get more insights on the system performance. Power optimization model was proposed based on the asymptotic results to enhance the system performance. The results showed that the SU network might operate efficiently at low to medium SNR values relative to the allowable PU interference threshold. Moreover, the proposed power optimization model resulted in a significant improvement in the outage performance in the medium SNR region.

References

[1] F. Yang, J. Cheng, and T. A. Tsiftsis, "Free-space optical communication with non-zero Boresight pointing errors," *IEEE Trans. Commun.*, vol. 62, no. 2, pp. 713–725, Feb. 2014.

[2] L. R. Varshney, "Transporting information and energy simultaneously," in *Proc. IEEE Int. Symp. Inf. Theory*, Toronto, ON, Canada, Jul. 2008, pp. 1612–1616.

[3] Z. Ding *et al.*, "Application of smart antenna technologies in simultaneous wireless information and power transfer," *IEEE Commun. Mag.*, vol. 53, no. 4, pp. 86–93, Apr. 2015.

[4] B. V. Nguyen, H. Jung, D. Har, and K. Kim, "Performance analysis of a cognitive radio network with an energy harvesting secondary transmitter under Nakagami-m fading," *IEEE Access*, vol. 6, pp. 4135–4144, 2018.

[5] C. Zhai, J. Liu, and L. Zheng, "Relay-based spectrum sharing with secondary users powered by wireless energy harvesting," *IEEE Trans. Commun.*, vol. 64, no. 5, pp. 1875–1887, May 2016.

[6] Y. Gao, H. He, Z. Deng, and X. Zhang, "Cognitive radio network with energy-harvesting based on primary and secondary user signals," *IEEE Access*, vol. 6, pp. 9081–9090, 2018.

[7] L. Yang, X. Gao, and M.-S. Alouini, "Performance analysis of relay assisted all-optical FSO networks over strong atmospheric turbulence channels with pointing errors," *IEEE/OSA J. Lightw. Technol.*, vol. 32, no. 23, pp. 4613–4620, Dec. 2014.

[8] I. S. Ansari, F. Yilmaz, and M-S. Alouini, "Performance analysis of free space optical links over Málaga-$\mathcal{M}$ turbulence channels with pointing errors," *IEEE Trans. Wireless Commun.*, vol. 15, no. 1, pp. 91–102, Jan. 2016.

[9] E. Soleimani-Nasab and M. Uysal, "Generalized performance analysis of mixed RF/FSO cooperative systems," *IEEE Trans. Wireless Commun.*, vol 15, no. 1, pp. 417–727, Sep. 2016.

[10] N. T. P. Van, S. F. Hasan, X. Gui, S. Mukhopadhyay, and H. Tran, "Three-step two-way decode-and-forward relay with energy harvesting," *IEEE Commun. Lett.*, vol. 21, no. 4, pp. 857–860, Apr. 2017.

[11] F. Li, H. Jiang, R. Fan, and P. Tan, "Optimal cooperative strategy in energy harvesting cognitive radio networks," in *Proc. IEEE Veh. Technol. Conf.*, Toronto, ON, Canada, Sep. 2017, pp. 1–6.

[12] F. Zhang, T. Jing, Y. Huo, and K. Jiang, "Throughput optimization for energy harvesting cognitive radio networks with save-then-transmit protocol," *Comput. J.*, vol. 60, no. 6, pp. 911–924, Jun. 2017.

[13] O. Elnahas, M. Elsabrouty, O. Muta, and H. Furukawa, "Game theoretic approaches for cooperative spectrum sensing in energy-harvesting cognitive radio networks," *IEEE Access*, vol. 6, pp. 11086–11100, 2018.

[14] M. Xu, M. Jin, Q. Guo, and Y. Li, "Multichannel selection for cognitive radio networks with RF energy harvesting," *IEEE Wireless Commun. Lett.*, vol. 7, no. 2, pp. 178–181, Oct. 2018.

[15] H. Liang, X. Zhao, and W. Zhang, "Optimal power allocations for multichannel energy harvesting cognitive radio," in *Proc. IEEE Int. Symp. World Wireless, Mobile Multimedia Netw.*, Macau, Jun. 2017, pp. 1–6.

[16] S. Yin, Z. Qu, and S. Li, "Achievable throughput optimization in energy harvesting cognitive radio systems," *IEEE J. Sel. Areas Commun.*, vol. 33, no. 3, pp. 407–422, Mar. 2015.

[17] G. Han, J. K. Zhang, and X. Mu, "Joint optimization of energy harvesting and detection threshold for energy harvesting cognitive radio networks," in *Proc.IEEE/CIC Int. Conf. Commun.*, Chengdu, China, Jul. 2016, pp. 1–5.

[18] N. P. Le, N. S. Vo, and M. T. Hoang, "Unified analysis of energy harvesting-based MIMO relay wireless systems over Nakagami-m fading channels,"*Trans. Emerg. Telecommun. Technol.*, vol. 28, no. 10, pp. 1–18, Oct. 2017.

[19] M. Trigui, N. Cherif, and S. Affes, "Relay-assisted mixed FSO/RF systems over Málaga-$\mathcal{M}$ and $\kappa - \mu$ shadowed fading channels," *IEEE Wireless Commun. Lett.*, vol 6, no. 5, pp. 682–685, Jul. 2017.

[20] I. Trigui, N. Cherif, S. Affes, X. Wang, V. Leung, and A. Stephenne, "Interference-limited mixed Málaga-$\mathcal{M}$ and Generalized-$\mathcal{K}$ dual-hop FSO/RF systems," in *Proc. IEEE Annu. Int. Symp. Pers., Indoor, Mobile Radio Commun.*, Montreal, QC, Canada, Oct. 2017, pp. 1–6.

[21] C. Abou-Rjeily, "Performance analysis of up-link and down-link mixed RF/FSO links with multiple relays," in *Proc. Int. Conf. Softw., Telecommun. Comput. Netw.*, Split, Croatia, Sep. 2017, pp. 1–6

[22] H. Arezumand, H. Zamiri-Jafarian, and E. Soleimani-Nasab, "Outage and diversity analysis of underlay cognitive mixed RF-FSO cooperative systems," *IEEE/OSA J. Opt. Commun. Netw.*, vol. 9, no. 10, pp. 909–920, Oct. 2017.

[23] F. S. Al-Qahtani, A. H. A. El-Malek, I. S. Ansari, R. M. Radaydeh, and S. A. Zummo, "Outage analysis of mixed underlay cognitive RF MIMO and FSO relaying with interference reduction," *IEEE Photon. J.*, vol. 9, no. 2, Apr. 2017, Art. no. 7902722.
[24] N. Varshney and A. K. Jagannatham, "Cognitive decode-and-forward MIMO RF/FSO cooperative relay networks," *IEEE Commun. Lett.*, vol. 21, no. 4, pp. 893–896, Apr. 2017.
[25] N. Varshney and P. Puri, "Performance analysis of decode-and-forward-based mixed MIMO-RF/FSO cooperative systems with source mobility and imperfect CSI," *IEEE/OSA J. Lightw. Technol.*, vol. 35, no. 11, pp. 2070–2077, Jun. 2017.
[26] N. Varshney, A. K. Jagannatham, and P. K. Varshney, "Cognitive MIMO-RF/FSO cooperative relay communication with mobile nodes and imperfect channel state information," *IEEE Trans. Cogn. Commun. Netw.*, vol. 4, no. 3, pp. 544–555, Sep. 2018.
[27] I. A. Alimi, P. P. Monteiro, and A. L. Teixeira, "Analysis of multiuser mixed RF/FSO relay networks for performance improvements in cloud computing-based radio access networks (CC-RANs)," *Opt. Commun.*, vol. 402, pp. 653–661, Nov. 2017.
[28] N. Varshney, P. K. Sharma, and M.-S. Alouini, "Opportunistic scheduling in underlay cognitive radio based MIMO-RF/FSO networks," May 2018, arXiv:1805.08943. [Online]. Available: https://arxiv.org/abs/1805.08943
[29] I. Alimi, A. Shahpari, V. Ribeiro, N. Kumar, P. Monteiro, and A. Teixeira, "Optical wireless communication for future broadband access networks," in *Proc. IEEE Eur. Conf. Netw. Opt. Commun.*, Lisbon, Portugal, Jun. 2016, pp. 124–128.
[30] Q. Fan *et al.*, "Reducing the impact of handovers in ground-to-train free space optical communications," *IEEE Trans. Veh. Technol.*, vol. 67, no. 2, pp. 1292–1301, Feb. 2018.
[31] H. Khanna, M. Aggarwal, and S. Ahuja, "Further results on the performance improvement in mixed RF-FSO systems using hybrid DF/AF (HDAF) relaying," *Trans. Emerg. Telecommun. Technol.*, vol. 29, no. 6, pp. 1–18, Feb. 2018.
[32] I. S. Ansari, M. M. Abdallah, M. S. Alouini, and K. A. Qaraqe, "Outage analysis of asymmetric RF-FSO systems," in *Proc. IEEE Veh. Technol. Conf.*, Montreal, QC, Canada, Sep. 2016, pp. 1–6.
[33] Wolfram, "The Wolfram functions site," 2013. [Online]. Available: http://functions.wolfram.com
[34] I. S. Gradshteyn and I. M. Ryzhik, *Tables of Integrals, Series and Products*, 6th ed. San Diago, CA, USA: Academic, 2000.
[35] D. B. da Costa and S. Aissa, "Cooperative dual-hop relaying systems with beamforming over Nakagami-m fading channels," *IEEE Trans. Wireless Commun.*, vol. 8, no. 8, pp. 3950–3954, Aug. 2009.
[36] A. Abu-Dayya and N. Beaulieu, "Outage probabilities of cellular mobile radio systems with multiple Nakagami interferers," *IEEE Trans. Veh. Technol.*, vol. 40, no. 4, pp. 757–768, Nov. 1991.
[37] A. J. Navas, J. M. G. Balsells, J. F. Paris, and A. P. Notario, "A unifying statistical model for atmospheric optical scintillation," in *Numerical Simulations of Physical and Engineering Processes*, J. Awrejcewicz, Ed. Rijeka, Croatia: Intech, 2011.
[38] M. K. Simon and M.-S. Alouini, *Digital Communication Over Fading Channels*, 2nd ed. Hoboken, NJ, USA: Wiley, 2005.
[39] T. A. Tsiftsis, H. G. Sandalidis, G. K. Karagiannidis, and N. C. Sagias, "Multihop free-space optical communications over strong turbulence channels," in *Proc. IEEE Int. Conf. Commun.*, Istanbul, Turkey, Jun. 2006, pp. 2755–2759.